Journal of Thermal Analysis and Calorimetry, Vol. 86 (2006) 2, 403–410

# THERMAL ANALYSIS AND ELECTROCHEMICAL STUDY OF Hg REACTIONS ON Pt–30% Ir ALLOY ELECTRODE

*E. Milaré, J. R. Turquetti, G. R. Souza, A. V. Benedetti and F. L. Fertonani*[*]

Instituto de Química, Universidade Estadual Paulista, Araraquara, São Paulo, C.P. 355, CEP 14.801-970, Brazil

Thermogravimetry (TG), cyclic voltammetry (CV) and other analytical techniques were used to study the reactions of mercury with Pt–30% Ir alloy. The results allowed to suggest that an electrodeposited mercury film interacts with the substrate and when subjected to heat or electrochemical removal at least four mass loss steps or five peaks appeared during the mercury desorption process. The first two steps were attributed to Hg(0) removal probably from the bulk and from the adsorbed monolayer which wets the electrode surface. These two processes are responsible for peaks D and F in the cyclic voltammograms. The last two peaks (G, H) in CV were ascribed to the intermetallic compound decomposition. In TG curves, the last two steps were attributed to the $PtHg_4$ (third step), and $PtHg_2$ decomposition followed by Hg removal from the subsurface. The $PtHg_2$ was formed by an eutectoide reaction: $PtHg \rightarrow PtHg_2+Hg(Pt–Ir)$. The Hg diffused to the subsurface was not detectable by cyclic voltammetry.

***Keywords:*** *alloy, cyclic voltammetry, SXR, thermogravimetry*

## Introduction

Pure platinum, rhodium and iridium, and platinum-iridium and platinum-rhodium alloys have been widely used to prepare microelectrodes [1–7], and catalysts used in petroleum-cracking industry [8, 9]. It is well known that when solid metals are placed in contact with liquid metals, a variety of physicochemical changes may occur, e.g., complete or partial solution of the solid, intermetallic compounds formation at the liquid-solid interface or in the solution, grain boundary grooving, and liquid metal embrittlement. Such changes may also cause structural deterioration of the solid surface [1–7].

Considering the importance of developing new substrates with high resistance to mercury amalgamation Pt–20% Ir alloy has been suggested as an appropriate substrate for mercury deposition because its surface is not apparently scarred by interaction with mercury [7]. However, intermetallic compounds such as $PtHg_4$ and $PtHg_2$ on the Pt–20% Ir alloy surface were identified based on X-ray diffraction results [4]. The changes in the surface morphology were investigated by optical interferometry and SEM, and changes in the energies of Hg and noble metals alloys interactions by XPS. The XPS results were interpreted considering a model where the electrode/solution interphase was composed by different phases including a three-layered region structure, containing at least two Pt–Hg intermetallics: $PtHg_4$ and $PtHg_2$, and a substrate modified region, enriched in iridium [4].

Nolan and Kounaves [10] have been prepared screen-printed Ir–Hg electrodes by deposition of iridium on silica wafer using sputtering. In this device, iridium was used due to its low solubility in mercury and very low chemical reactivity with mercury [11]. However, it was observed that when the stripping process to Hg removal was applied the electrode surface area increased as a consequence of the mercury-iridium interactions which deteriorated the electrode surface [5, 10, 12, 13].

In our laboratories, preliminary studies involving Pt–30% Rh alloy has suggested the formation of $PtHg_2$ and $RhHg_2$ intermetallic compounds. The absence of $PtHg_4$ compound was attributed to the interference of the intermetallic $RhHg_2$ which could induce the formation of isostructurals compounds containing two Hg atoms. The formation of a diffusion barrier of Rh could difficult the permeation of Hg into the substrate underlayer [14]. For a better understanding of the mercury action on Pt–30% Ir alloy surface a comparative study using thermal analysis and electrochemical techniques was planed. Therefore, in this work, mercury films were electrodeposited on Pt–30% Ir foils, and mercury desorption was investigated by thermogravimetry/differential thermogravimetry (TG/DTG), differential scanning calorimetry (DSC), and cyclic voltammetry (CV), varying the scan rate and Hg(I) ions concentration into the solution. The new surfaces generated at the end of each mass loss step in TG curves, and at the end of each oxidation peaks, were analysed using energy dispersive

* Author for correspondence: fertonan@iq.unesp.br

*1388–6150/$20.00*

*Akadémiai Kiadó, Budapest, Hungary*
*Springer, Dordrecht, The Netherlands*

X-ray microanalysis (EDX), scanning electron microscopy (SEM), surface mapping and X-ray diffractometry (XRD).

## Experimental

Pt–30% Ir foils (Heraeus Vectra) were polished with $\alpha$-$Al_2O_3$ (particles size <0.3 μm) (Buehler) aqueous suspension and sonicated in $HNO_3$:$H_2O$ (50% v/v) solution. Suprapure acids (Merck) and Milli-Q water of 18 M Ω cm were used. Afterwards a mercury film was deposited on the foils used in the TG and DSC analysis. For mercury film deposition an Ecochemie Potentiost-Galvanostat PGSTAT10 and a washing electrochemical cell (10 mL) to allow matrix solution exchange were used. A Pt–30% Ir foil (geometric area 65 $mm^2$) was used as working electrode. A large platinum gauze (around 1 $cm^2$) (Heraeus Vectra) was the counter-electrode and an Ag|AgCl|$KNO_{3(sat)}$, $AgCl_{(sat)}$ the reference electrode. This reference was used to substitute the double junction electrode to avoid $Hg_2Cl_2$ precipitation at the junction for long time experiments. Firstly, a cyclic voltammogram in the supporting electrolyte solution with $E_{initial}$=$E_{final}$= 0.6 V; $E_{\lambda,1}$= –0.22 V and $E_{\lambda,2}$=1.02 V, at 50 mV $s^{-1}$ was recorded. Afterwards, the mercury was deposited from a degassed and quiescent solution containing $6.15\cdot10^{-2}$ mol $dm^{-3}$ mercurous ions, applying –0.75 V for 300 s. Then, TG and DSC experiments were performed using foils with mercury electrodeposited. TG curves (TG-50) were recorded from 30 to 800°C and DSC curves (DSC-25) from 30 to 250°C, both at 5°C $min^{-1}$ under a purified $N_2$ flux (150 $cm^3$ $min^{-1}$), using a Mettler Thermoanalyser TA4000 System.

For cyclic voltammetric studies the foils were polished and cleaned as above described. Then, the foils were submitted to electrochemical measurements in 1.00 mol $dm^{-3}$ $KNO_3/HNO_3$ (pH 1) or 1.00 mol $dm^{-3}$ $KNO_3/HNO_3$ (pH 1)/$5.86\cdot10^{-3}$ or $2.05\cdot10^{-4}$ mol $dm^{-3}$ Hg(I) solution prepared from a $C_{Hg(I)}$=$60.0\cdot10^{-3}$ mol $dm^{-3}$ stock solution. The electrodes, electrochemical cell and equipments were the same above described. The working electrode was a Pt–30% Ir (geometric area of 70 $mm^{-2}$). Single and consecutive cyclic voltammograms were performed at different scan rates and the inset in the figures shows the potential program applied.

Sample surfaces before and after to be heated up to different temperatures, and after electrochemical measurements were examined using JEOL JSM-T330A microscope coupled to a Noran system to obtain SEM images, mapping of the elements and EDX spectra. Also, XRD analyses were carried out using a diffractometer HIGAKU RINT 2000 with a rotatory anode ($K_{\alpha_{Cu}}$=1.54184 Å, step=0.05°, 20≤2θ≤120°), and data analyzed using AFPAR and DHKL softwares [15].

## Results and discussion

*Thermal analysis*

Figure 1 shows the TG curves for Pt–30% Ir/Hg system. The TG analysis suggested a mass loss process occurring in four steps. The first, a step with fast kinetic and occurring from 30 to ca. 140°C, was attributed to bulk Hg removal (Δ*m*=92.27%). Comparing these findings with those for Pt–20% Ir/Hg system [4] a significant increase in the quantity of bulk Hg lost was found for Pt–30% Ir (92%) *vs.* 80% for Pt–20% Ir. This result is coherent with a lower quantity of Hg interacting with the substrate containing 30% of Ir, since it is less reactive.

The second step, with a fast kinetic and occurring from ca. 140 to ca. 160°C, was attributed to the removal of Hg which is wetting the Pt–Ir alloy surface (Δ*m*=3.82%).

The third step, of relatively slow kinetic, and occurring from ca. 160 to ca. 240°C, was attributed to thermal decomposition of $PtHg_4$ intermetallic compound (Δ*m*=1.53%). The XRD data (Table 1) proves the presence of $PtHg_4$, which is stable at least up to 180°C.

The fourth step of TG curve, occurring with a slow kinetic from ca. 240 to ca. 650°C, was attributed to $PtHg_2$ decomposition and Hg removal from the subsurface of the Pt–Ir alloy (Δ*m*=1.82%). The $PtHg_2$ compound was only detected when the Pt–Ir–Hg foil was heated up to 240°C, and not when the sample was heated up to 180°C, as indicated in Table 1.

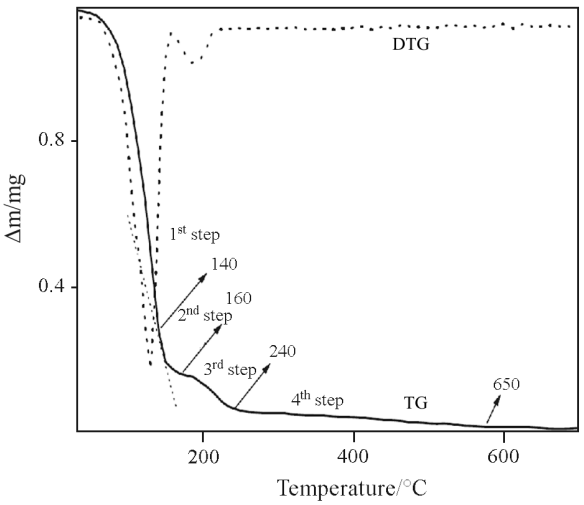


**Fig. 1** TG and DTG curves obtained for Pt–30% Ir/Hg from 30 to 700°C; β=5°C $min^{-1}$; $N_2$ flux= 150 mL $min^{-1}$. Initial mass of mercury, $m_{iHg}$=1.15 mg Hg

**Table 1** XRD peaks obtained for Pt–Ir alloy foil surface heated up to 180°C. Ir and Hg theoretical 2θ values were obtained from an Ir prototype [18]

| Experimental | Theoretical | Compound |
|---|---|---|
| 20.25 | 20.30 | $PtHg_4$ |
| 21.50 | 21.34 | $PtO_2$ |
| 28.73 | 28.80 | HgO |
| 35.38 | 35.55 | $PtHg_4$ |
| 39.13 | 39.25 | $HgO_2$ |
| 40.16 | 40.67 | Ir |
| 46.79 | 46.42 | $PtHg_4$ |
| 68.28 | 68.28 | $HgO_2$ |
| 74.84 | 74.94 | $HgO_2$ |
| 82.07 | 82.25 | PtHg |
| 86.43 | 86.44 | HgO |
| 104.70 | 104.76 | HgO |
| 118.93 | 118.95 | HgO |

Now, the origin of $PtHg_2$ must be explained. In this system $PtHg_2$ was not originated from the $PtHg_4$ decomposition as observed for Pt–15% Rh [14] since $PtHg_2$ is not stable in the absence of the isostructural $RhHg_2$ compound and is only detected when produced by the PtHg decomposition via an eutectoide reaction: $PtHg \rightarrow PtHg_2+Hg$(Pt–Ir). PtHg and $PtHg_4$ are stable compounds as indicated by their presence in samples even heated up to 180°C (Table 1).

In a parallel experiment, the heating process was stopped at 240°C and the XRD showed only $PtHg_2$ which diminishes increasing the temperature. It is well known that Ir does not react with Hg to form intermetallic compounds [4, 5, 11, 16, 17]. So, it is probable that Ir takes no part in these processes, and the decomposition of PtHg compounds to give $PtHg_2$ and diffusion of Hg into the substrate, followed by $PtHg_2$ decomposition and Hg removal from the subsurface explaining the nature of the fourth mass loss step in TG curves.

Table 1 shows the XRD data obtained after submitting the sample to TG analysis. Mercury oxides and, $PtHg_4$ and PtHg intermetallic compounds were detected. The presence of $PtHg_4$ and the absence of $PtHg_2$ could be attributed to the fact that Ir does not form intermetallic compounds with Hg as Rh, and so $PtHg_2$ is not stabilized on Pt–Ir alloy.

Figure 2 shows the DSC curve recorded immediately after Hg electrodeposition, from 30 to 250°C in the same experimental conditions of TG curves. It shows two consecutive endothermic peaks at 142°C (peak A) and 157°C (peak B) attributed respectively to Hg removal from the bulk and from adsorbed layer of Hg that is wetting the Pt–Ir surface. This result confirms the attribution gave for the first and second steps of TG curve (Fig. 1).

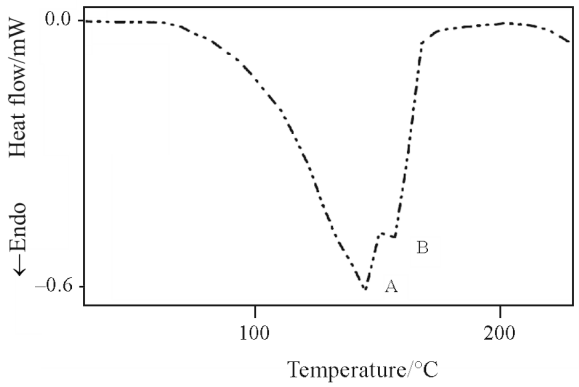


**Fig. 2** DSC curve obtained to Pt–30% Ir/Hg system from 30 to 250°C; β=5°C $min^{-1}$; $N_2$ flux=150 mL $min^{-1}$. Aluminium pan

Although pure Ir does not form intermetallic compounds its surface was scratched by interaction with Hg, and so Ir surface is modified by the presence of Hg [5]. The Pt–30% Ir alloy reacts with Hg forming Pt–Hg intermetallic compounds, however the amount of these compounds diminishes as the Ir content increases [1, 4]. Another interesting result was the embrittlement of the Pt–30% Ir alloy surface after Hg removal up to 700°C via TG analysis when compared with the original foil subjected to the same heat treatment.

*Cyclic voltammetry*

Figure 3 shows a cyclic voltammogram recorded for a laminar electrode of Pt–30% Ir alloy, in 1.00 mol $cm^{-3}$ $KNO_3/HNO_3$ (pH 1) solution, in the potential range between hydrogen and oxygen evolution reactions. Three peaks were observed: peak A, in the cathodic scan, attributed to the reduction of PtO-containing species, and peaks F and H attributed

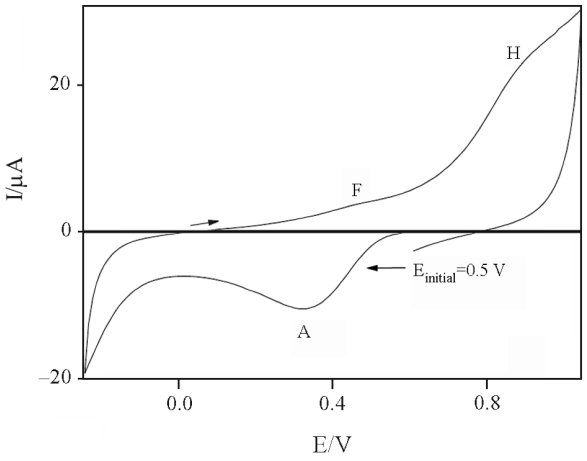


**Fig. 3** Cyclic voltammogram for Pt–30% Ir alloy in 1 mol $dm^{-3}$ $KNO_3/HNO_3$ (pH 1) solution, at 0.05 V $s^{-1}$

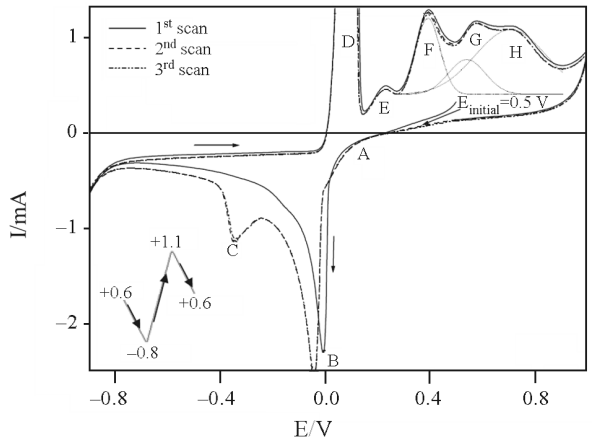


**Fig. 4** Consecutive cyclic voltammograms for Pt–30% Ir–Hg electrode in 1 mol $dm^{-3}$ $KNO_3/HNO_3$ (pH 1)+ $5.86 \cdot 10^{-3}$ mol $dm^{-3}$ [Hg(I)] solution, at 0.05 V $s^{-1}$

to the formation of IrO- [19] and PtO-containing species [20] respectively, and the hydrogen evolution was observed at around –0.25 V.

Figure 4 shows cyclic voltammograms recorded for a laminar electrode of Pt–30% Ir alloy in the supporting electrolyte without and with Hg(I)-containing solution ($C_{Hg(I)}=5.86 \cdot 10^{-3}$ mol $dm^{-3}$), at 0.050 V $s^{-1}$. At the initial potential (+0.6 V) an anodic current was observed, which was related to the oxidation of Hg underpotentially deposited under open-circuit condition. It is well known that underpotential deposition of Hg on Pt and Ir occurs [5, 12, 17]. In the present work, it was also observed that the open-circuit potential varied with time, probably due to surface modifications caused by the interaction with Hg. The surface modifying was also denounced by the shifting of cathodic potential limit for hydrogen (HER) evolution reaction, which changes from around –0.25 V in absence or very low mercury ions concentration to –0.80 V in $C_{Hg(I)}=5.86 \cdot 10^{-3}$ mol $dm^{-3}$ solution. The Hg interaction with the surface producing intermetallic compounds and mercury diffusion into the noble alloy were responsible by shifting the hydrogen evolution. Following the cathodic scan three peaks were observed: a bad defined peak A ($E$=+0.1 V) attributed to the mercury underpotential deposition (UPD) together with O-containing species reduction; peak B ($E$= –0.03 V) attributed to bulk Hg deposition; and peak C ($E$= –0.34 V) attributed to the formation of intermetallic compounds. In the anodic scan five peaks were observed: peak D ($E$=+0.08 V) attributed to the bulk Hg removal [1, 4–6, 17]; peak E ($E$=+0.23 V) attributed to oxidation of adsorbed Hg(I) to Hg(II) on the modified substrate [4, 5, 17]; peak F ($E$=+0.39 V) attributed to the oxidation of a Hg thin film [5, 17] and Ir oxides formation [19]; peak G ($E$=+0.58 V) attributed to the decomposition of PtHg intermetallic compound [1, 4, 14] and the formation of PtO-containing species [1, 4]; peak H ($E$=+0.72 V) attributed to $PtHg_4$ intermetallic compounds decomposition [4] and PtO-containing species formation. The $PtHg_4$ and PtHg intermetallic compounds were confirmed by X-ray diffractometry (data not shown). Peaks F, G and H were better distinguished using peaks deconvolution procedures (Fig. 4).

Figure 4 also shows the second and third scans indicating very similar I–E profiles to the first scan, except that the charge related with peak C is higher than that for the first scan. This increase in peak C can be ascribed to the Pt enrichment at the electrode surface, which allows increasing the $PtHg_4$ and PtHg formation. The mercury removal from Hg film and intermetallic compounds allowed the electrode surface to be Pt-enriched since Pt was not dissolved at this potential range (no Pt was detected in the solution by inductively coupled plasma atomic emission, ICP-AE). A similar peak was also observed for Pt–20% Ir–Hg system [4].

After recording cyclic voltammograms in the presence of Hg, Pt–Ir electrodes became brittle compared to the originals, probably due to the diffusion of Hg into the Pt alloy lattice, causing its expansion, Hebbinder effect [21]. This observation is in agreement with the results obtained by thermal analysis ('Thermal analysis').

Comparing these cyclic voltammograms (Fig. 4) with those obtained for Pt–20% Ir alloy (Fig. 1, [4]) one can observe that the anodic peak potentials were shifted to less positive values for Pt–30% Ir–Hg, suggesting a decrease in the substrate reactivity due to the weaker interaction of Hg with iridium richer substrate.

Figure 5 shows the influence of stirring on I–E profiles consecutively recorded in a solution containing lower mercury (I) concentration ($2.05 \cdot 10^{-4}$ mol $dm^{-3}$). Figure 5a shows the profile of the cyclic voltammograms obtained immediately after immersing the Pt–30% Ir electrode in a deaerated Hg(I)-containing solution ($C_{Hg(I)}=2.05 \cdot 10^{-4}$ mol $dm^{-3}$). At the first scan (beginning at +0.45 V) the initial current was positive probably due to the oxidation of a little quantity of Hg deposited via UPD. Following the cathodic scan, peak B (at around 0.2 V) was attributed to the Hg deposition and PtO species reduction and peak C is not significant. In the reverse scan, peak D is very low suggesting that the bulk mercury was mainly used to form intermetallic species; the absence of peak F was related to the very low intensity of peak D (low quantity of bulk Hg) and corroborates the attribution given to the peak F in Fig. 4. Peaks G and H have the same attribution given in Fig. 4. Also, no significant differences among the consecutive cyclic voltammograms were observed.

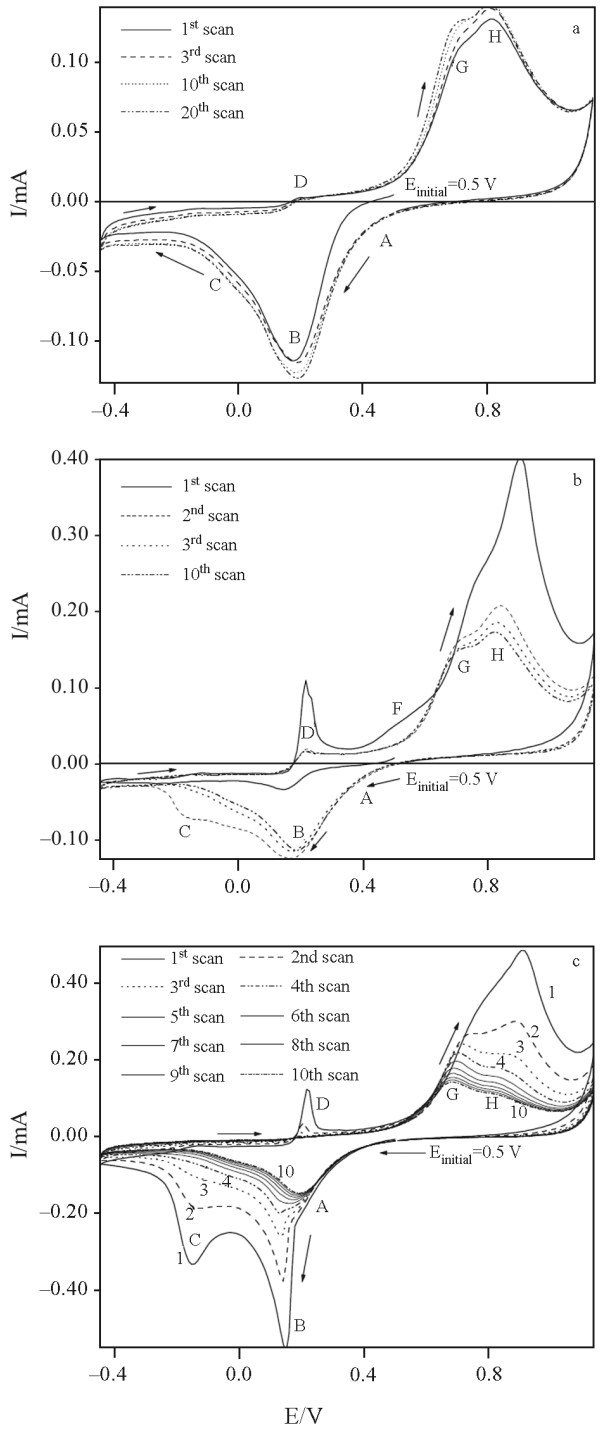


**Fig. 5** Consecutive cyclic voltammograms for the system Pt–30% Ir/Hg obtained in Hg(I)-containing solution (1 mol $dm^{-3}$ $KNO_3$, pH 1, $HNO_3$, $C_{Hg(I)}=2.05\cdot10^{-4}$ mol $dm^{-3}$), $v$=0.05 V $s^{-1}$. a – without, b – with and c – without agitation

Immediately after recording Fig. 5a, the solution was stirred for 20 min using a $N_2$ flux and maintaining the same electrode used in Fig. 5a, at open-circuit potential. Then, I–E profiles were consecutively registered, at 0.05 V $s^{-1}$ and under stirring (Fig. 5b). At the first scan an increase of peaks D, G and H was observed, and peak F appeared. Also, peak B showed low intensity due to the decreasing in Hg concentration into the solution during the open circuit potential, caused by the UPD process. At the same condition peak C was not clearly observed at the first scan, suggesting that the intermetallic compounds could be formed during Hg accumulation at open circuit potential. These events corroborate the response observed at the first anodic scan. In the subsequent scans the I–E profiles were close to those of Fig. 5a, since the concentration of Hg into the solution was almost reestablished during the anodic scan, and also because the overall process is surface-controlled. It should be noted that overlapping the effects of mass transport by stirring the solution, the surface is being continuously modified by the repetitive potential scans, mainly reflected by the Pt enrichment at the electrode surface [1, 4, 6, 14], which also contributes to change the I–E profile.

The nitrogen flux was stopped and after 20 min at quiescent condition and at open circuit the I–E profiles were recorded (Fig. 5c). Then, the experimental condition in Fig. 5c was the same as in Fig. 5a, except that the electrode had been submitted to 32 cycles under different conditions (Figs 5a and b). In the first cathodic scan peaks B and C in Fig. 5c were well defined and showed higher intensity compared with these peaks in Figs 5a and b. The surface modification occurred during the prior experiments and the quiescent solution condition could be responsible by the changes observed in this first scan. In the first anodic scan, peaks D, G and H were clearly observed and peak F was not detected. Peaks D, G and H were dependent on peaks B and C, and the difference in charge of peaks B and D was related to the Hg consumption to form intermetallic compounds (peak C). Initially, peak H continuous being higher than peak G, probably due to the combined effect of Pt enrichment at the surface and the higher quantity of Hg at the electrode, which allowed a preferential formation of $PtHg_4$ (peak H). In the subsequent scans all peaks decreased due to the difficult in recomposing Hg ions concentration near the electrode surface, increasing the thickness of the diffusion layer. Finally, it was observed that peak H became lower than G after the second or third cycles (Fig. 5c). This result can be attributed to the Pt-enrichment at the electrode surface during the total cycling and the increase of surface area favoring the increase of PtHg film (peak G) in detriment of $PtHg_4$ formation (peak H). The results indicate that the consecutive cycling causes irreversible damages to the substrate.

Comparing cyclic voltammograms recorded for pure Ir [12] in Hg(I)-containing solution and recorded

under the same conditions used for Pt–30% Ir showed that the Pt nature dominates the electrochemical response of Pt–Ir alloys even at high Ir content.

The interdependence among anodic peaks was studied holding the potential at the end of each peak up to the current decreased to a value near zero and restarting the scan again (Fig. 6). I–E profile of peaks after holding the potential at different values was not significantly modified suggesting certain independence among anodic peaks.

The behavior of peak H was also studied recording cyclic voltammograms (not shown) in $C_{Hg(I)}=2.05\cdot10^{-4}$ mol dm$^{-3}$ solution at different scan rates: $0.00125\leq v\leq0.3$ V s$^{-1}$. Figure 7 shows a linear correlation of $I_p=f(v)$ for the peak H, indicating an adsorptive control, as expected for redox processes involving species present at the electrode surface. Using larger Hg(I) ions concentration, studies accomplished with solution matrix exchange confirmed this assumption. For matrix exchanging experiments the following procedure was used: (1) a complete cyclic voltammogram was recorded in presence of Hg ions and afterwards the potential was held at 0 V and the solution was changed by the supporting electrolyte without Hg ions; (2) the sweeping was restarted scanning the potential from 0.0 to 0.3 V (to remove the bulk Hg deposited), holding this potential applied up to I=0 A was attained, and a new matrix exchanging was done; (3) the sweeping potential was starting again to record the potential region corresponding to peak H. After this procedure, peak H was still present confirming its correspondence to the oxidation of $PtHg_4$.

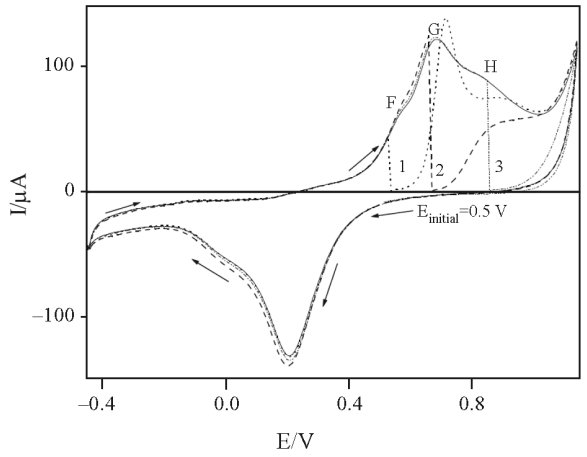


**Fig. 6** Cyclic voltammograms holding the potential at different potential values up to the condition of $I$=0 A: 1 – $E$=0.53 V; 2 – $E$=0.67 V; 3 – $E$=0.85 V. $C_{Hg(I)}=2.05\cdot10^{-4}$ mol dm$^{-3}$; $v$=0.05 V s$^{-1}$

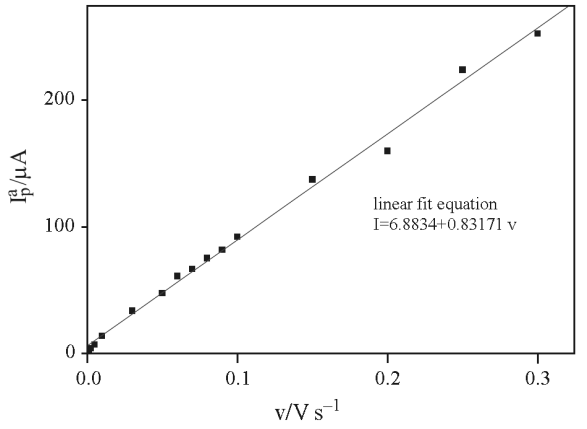


**Fig. 7** $I_p^a$ *vs.* $v$ plot for Pt–30% Ir/Hg system. $C_{Hg(I)}=2.05\cdot10^{-4}$ mol dm$^{-3}$; $0.00125\leq v\leq0.3$ V s$^{-1}$ following the procedure above described

X-ray diffractometry performed after matrix exchanging showed a large amount of $PtHg_4$ intermetallic compound, and lower quantity of PtHg, besides a small amount of HgO oxides and PtO-containing species. This experiment corroborates the electrochemical results.

Comparing TG and cyclic voltammetric results it was possible to suggest a correlation between TG steps and cyclic voltammetric peaks: the first and second steps in TG curve were linked to peaks D and F, attributed to the removal or oxidation of bulk Hg and Hg wetting the Pt–Ir alloy surface, respectively, and; the third step of TG curve was linked to peaks G and H attributed to intermetallic compounds decomposition. The fourth step in TG curve does not present the corresponding peaks in cyclic voltammograms, because the Hg presents in sublayers of substrate was only removed by heating at high temperature (800°C). It is very difficult to remove this mercury by potential applying, even after 2 h of controlled potential electrolysis at around +0.9 V. Peak E, appearing in cyclic voltammogram, did not have correspondent in TG curves because it was attributed to the oxidation of adsorbed Hg(I) to Hg(II) ions.

### *Scanning electron microscopy and surface analysis*

SEM images (Figs 8a and 9b) obtained at the end of the second step (180°C) and at the end of the TG curve (800°C) reveal a significant degradation of the substrate surface with the increase of temperature. The mapping of elements revealed a homogeneous Hg distribution on the substrate surface, which is related with the Hg wetting properties, low contact angle that allows Hg to wet completely the alloy surface.

Figures 9b and d show the alloy surface after almost complete Hg removal by heating up to 800°C and the free-mercury control sample submitted to the same temperature. A higher surface degradation was observed for the sample from which the Hg was completely removed by heating, while the control showed no appreciable changes.

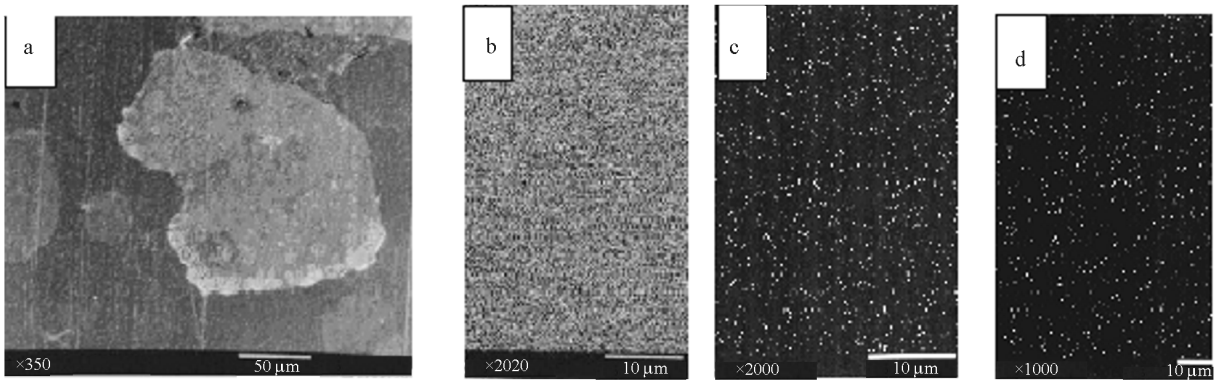


**Fig. 8** SEM images and mapping of elements for samples heated up to 180°C: a – SEM images; b – Pt mapping; c – Ir mapping; d – Hg mapping. $E_{beam}$=30 kV

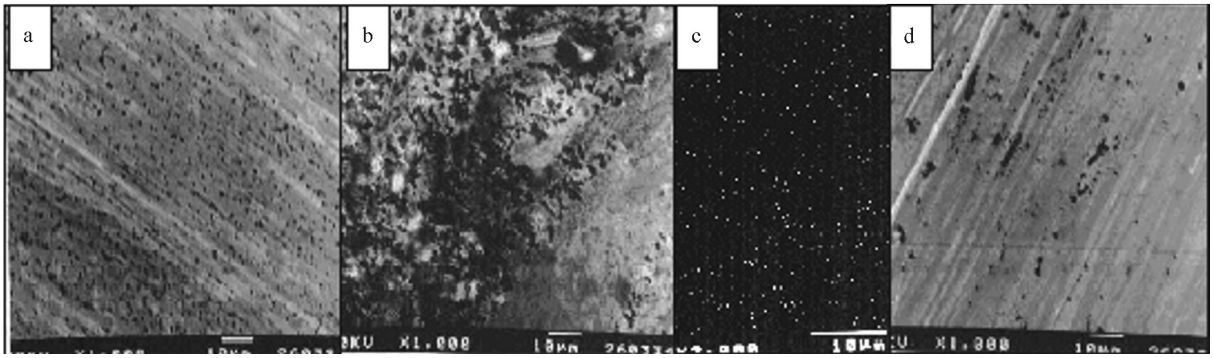


**Fig. 9** SEM images of Pt–30% Ir/Hg: a – control sample; b – sample heated up to 800°C (heating rate: 5°C $min^{-1}$; $N_2$ flux=150 mL $min^{-1}$); c – Hg mapping of sample b ($E_{beam}$=30 kV); d – control sample without electrodeposited Hg and heated up to 800°C under the same experimental conditions as b. Magnification: a –; b –; and d – 1000X; c – 2000X

It is interesting to note that the presence of Hg on the alloy surface was detected even after heating up to 800°C for all the following Hg-systems: Pt–30% Ir (Fig. 9c), Pt–10% Rh [1, 2], Pt–30% Rh [13] and Pt–20% Ir [1, 12] alloys, while Pt–Hg system when heated up to the same temperature, showed no Hg in the element mapping [1].

For electrochemical mercury removal applying a constant potential of +0.3 V (Fig. 4) the mapping of elements (not shown) confirmed the homogeneous distribution of Hg all over the alloy surface, as it was observed after thermal removal at 180°C.

The surface roughness increased as the mercury was being removed, especially by heating, as confirmed by the scratching of the surface, and both grain and grain boundaries were attacked by Hg, resulting in a homogeneous Hg distribution on the alloy surface. A less pronounced attack to the surface was verified when Hg was removed by cyclic voltammetry.

## Conclusions

SEM, X-ray and cyclic voltammograms results obtained for Pt–30% Ir–Hg system allowed to identify Pt-mercury intermetallic compounds formation, but no Ir–Hg compounds were detected. The Hg removal by heating or electrochemical method occurred via several steps, beginning by removal the bulk mercury, adsorbed mercury, intermetallic compounds ($PtHg_4$ and PtHg) decomposition and finally the Hg from the substrate subsurface. It was also concluded by the formation of a thin film of O-containing (PtO and HgO) species on the substrate. The surface roughness increased as the mercury was being removed, especially by heating, and a less pronounced attack to the surface was verified when Hg was removed by cyclic voltammetry.

In cyclic voltammograms the current peaks were more pronounced for Hg(I) ions concentration greater than $2.05 \cdot 10^{-4}$ mol $dm^{-3}$. At open circuit Hg deposited at underpotential condition modifying the reactivity of the electrode surface. For low concentration of Hg(I) ions in solution ($\leq 2.05 \cdot 10^{-4}$ mol $dm^{-3}$), the bulk mercury was almost totally used to form intermetallic compounds and the peak corresponding to bulk mercury oxidation almost disappeared, while those corresponding to the oxidation of intermetallic compounds were still present. Studies varying the sweep rate suggest an adsorptive behavior for $PtHg_4$ oxidation.

Consecutive cyclic voltammetry and Hg removal produced irreversible damage at the electrode surface. The mercury removal from Hg film and intermetallic compounds allowed the electrode surface to be Pt-enriched, and consecutive cycling in presence of Hg(I) ions in solution made Pt–Ir electrodes brittle compared to the originals, probably due to the diffusion of Hg into the Pt alloy lattice.

Comparing TG and cyclic voltammetric results it was possible to suggest a correlation between TG steps and cyclic voltammetric peaks. It is very difficult to remove the mercury corresponding to the fourth step in TG curve by electrolysis, even after 2 h at +0.9 V.

## Acknowledgements

The authors thank to Fundação de Amparo à Pesquisa do Estado de São Paulo (FAPESP) and Conselho Nacional de Desenvolvimento Científico e Tecnológico (CNPq) for scholarships and financial support.

## References

1 F. L. Fertonani, A. V. Benedetti and M. Ionashiro, Thermochim. Acta, 265 (1995) 151.
2 F. L. Fertonani, M. Ionashiro, P. Melnikov, F. Sanz and A. V. Benedetti, Proceedings of XII Congreso Iberoamericano y IX Encontro Venezolano de Electroquimica, Merida, Venezuela 1996, p. 416.
3 E. Milaré, F. L. Fertonani, M. Ionashiro, A. V. Benedetti and P. Melnikov, Proceedings of XIII Congreso de la Sociedad Iberoamericana de Electroquimica, Viña del Mar 1998, p. 140.
4 F. L. Fertonani, A. V. Benedetti, J. Servat, J. Portillo and F. Sanz, Thin Solid Films, 341 (1999) 147.
5 F. L. Fertonani, E. Milaré, A. V. Benedetti and M. Ionashiro, J. Therm. Anal. Cal., 67 (2002) 403.
6 E. Milaré, F. L. Fertonani, M. Ionashiro and A. V. Benedetti, J. Therm. Anal. Cal., 59 (2000) 617.
7 C. Wechter and J. Osteryoung, Anal. Chem. Acta, 234 (1990) 275.
8 R. W. Joyner and E. S. Shpiro, Catal. Lett., 9 (1991) 239.
9 M. Barlow and P. J. Planting, Z. Metallkd., 60 (1969) 292.
10 M. A. Nolan and S. P. Kounaves, J. Electroanal. Chem., 453 (1998) 39.
11 S. P. Kounaves and J. Buffle, J. Electroanal Chem., 216 (1987) 53.
12 E. Milaré, E. Y. Ionashiro, Y. Maniette, A. V. Benedetti and F. L. Fertonani, Port. Electrochim. Acta, 21 (2003) 69.
13 E. Milaré, E. Y. Ionashiro, A. V. Benedetti and F. L. Fertonani, Port. Electrochim. Acta, 21 (2003) 155.
14 E. Y. Ionashiro and F. L. Fertonani, Thermochim. Acta, 383 (2002) 153.
15 B. Lestienne, B. Saux and R. Vdm, Complex des programme. France: CNRS, 1990.
16 C. Guminski, Bull. Alloy Phase Diagrams, 11 (1990) 22.
17 S. P. Kounaves and J. Buffle, J. Electrochem. Soc., 133 (1986) 2495.
18 International Centre For Diffraction Data. Powder Diffraction File: release 1999: data sets 1–49 plus 70–86: pdf. Pensylvania, 1999.
19 A. E. Bolzán, M. I. Florit and A. J. Arvía, J. Electroanal. Chem., 461 (1999) 40.
20 D. T. Sawyer, A. Sobkowiak and J. L. Roberts, Electrochemistry for Chemists, 2nd Edition, John Wiley & Sons, New York 1995.
21 E. D. Shchukin, I. V. Vidensky and V. I. Savenko, Coll. Surf. A - Physicochem. Eng. Asp., 142 (1998) 175.

Received: June 27, 2005
Accepted: June 16, 2006

DOI: 10.1007/s10973-005-7147-0